

## Detection of Non-Melanoma Skin Cancer by *in vivo* Fluorescence Imaging with Fluorocoxib A

Hyejun Ra<sup>\*,†</sup>, Emilio González-González<sup>\*,†</sup>,  
Md. Jashim Uddin<sup>¶,§,\*\*</sup>, Bonnie L. King<sup>\*,†</sup>,  
Alex Lee<sup>††</sup>, Irfan Ali-Khan<sup>\*,†</sup>, Lawrence J. Marnett<sup>¶,§,\*\*</sup>,  
Jean Y. Tang<sup>††</sup> and Christopher H. Contag<sup>\*,†,§</sup>

\*Molecular Imaging Program at Stanford (MIPS), Stanford University School of Medicine, Stanford, CA; <sup>†</sup>Dept. of Pediatrics, Stanford University School of Medicine, Stanford, CA; <sup>‡</sup>Dept. of Radiology, Stanford University School of Medicine, Stanford, CA; <sup>§</sup>Dept. of Microbiology & Immunology, Stanford University School of Medicine, Stanford, CA; <sup>¶</sup>A.B. Hancock Jr. Memorial Laboratory for Cancer Research, Department of Biochemistry, Vanderbilt University School of Medicine, Nashville, TN; <sup>#</sup>A.B. Hancock Jr. Memorial Laboratory for Cancer Research, Department of Chemistry, Vanderbilt University School of Medicine, Nashville, TN; <sup>\*\*</sup>A.B. Hancock Jr. Memorial Laboratory for Cancer Research, Department of Pharmacology, Vanderbilt University School of Medicine, Nashville, TN; <sup>††</sup>Department of Dermatology, Stanford University School of Medicine, Stanford, CA

### Abstract

Non-melanoma skin cancer (NMSC) is the most common form of cancer in the US and its incidence is increasing. The current standard of care is visual inspection by physicians and/or dermatologists, followed by skin biopsy and pathologic confirmation. We have investigated the use of *in vivo* fluorescence imaging using fluorocoxib A as a molecular probe for early detection and assessment of skin tumors in mouse models of NMSC. Fluorocoxib A targets the cyclooxygenase-2 (COX-2) enzyme that is preferentially expressed by inflamed and tumor tissue, and therefore has potential to be an effective broadly active molecular biomarker for cancer detection. We tested the sensitivity of fluorocoxib A in a BCC allograft SCID hairless mouse model using a wide-field fluorescence imaging system. Subcutaneous allografts comprised of 1000 BCC cells were detectable above background. These BCC allograft mice were imaged over time and a linear correlation ( $R^2 = 0.8$ ) between tumor volume and fluorocoxib A signal levels was observed. We also tested fluorocoxib A in a genetically engineered spontaneous BCC mouse model (Ptch1<sup>+/-</sup> K14-Cre-ER2 p53<sup>fl/fl</sup>), where sequential imaging of the same animals over time demonstrated that early, microscopic lesions (100  $\mu$ m size) developed into visible macroscopic tumor masses over 11 to 17 days. Overall, for macroscopic tumors, the sensitivity was 88% and the specificity was 100%. For microscopic tumors, the sensitivity was 85% and specificity was 56%. These results demonstrate the potential of fluorocoxib A as an *in vivo* imaging agent for early detection, margin delineation and guided biopsies of NMSCs.

*Neoplasia* (2015) 17, 201–207

### Introduction

Skin malignancies are traditionally classified as melanoma vs. nonmelanoma skin cancer (NMSC). NMSC is mainly comprised of two types: i) basal cell carcinoma (BCC), which is the most common type (~80% of all NMSC), evolves from basal epithelial cells in the epidermis and rarely metastasizes – but can invade the

Address all correspondence to: Christopher H. Contag, PhD, Clark Center, East Wing E150, 318 Campus Drive, Stanford University School of Medicine, Stanford, California 94305–5439.  
E-mail: ccontag@stanford.edu

Received 9 November 2014; Accepted 23 December 2014

© 2015 The Authors . Published by Elsevier Inc. This is an open access article under the CC BY-NC-ND license (<http://creativecommons.org/licenses/by-nc-nd/4.0/>).

1476-5586/15

<http://dx.doi.org/10.1016/j.neo.2014.12.009>

surrounding tissue if left untreated; ii) squamous cell carcinoma (SCC), a cancer of squamous epithelial cells, is less abundant (~20% of NMSC) but more aggressive. NMSC is the most common malignancy in the United States [1] as well as other reported countries [2]. NMSC is underestimated and often excluded from cancer statistics [3], although its prevalence more than doubles that of all other cancers combined [4] and its incidence continues to rise [1]. Despite a low mortality rate, the morbidity and cost associated with NMSC places it as the fifth most expensive cancer to treat overall in the Medicare population [1,5]. Early detection of skin cancer is the best way to improve patient outcome and reduce related costs, although it remains difficult in practice.

The current standard of care for skin cancer screening is visual inspection by primary care physicians or dermatologists, by the naked eye or using a dermascope, which heavily relies on medical experience. Other noninvasive systems have been investigated for skin cancer detection and classification, such as near-infrared reflectance confocal microscopes [6,7], which lack molecular specificity. Other approaches include the use of lesion-associated markers that can be fluorescently detected, such as protoporphyrin-IX (PpIX) detection after light exposure on areas incubated with the photodynamic therapy drug, 5-aminolevulinic acid (ALA) [8–11]. However, phototoxicity precludes its wider use for screening/diagnostic purposes on sun-exposed areas of the skin.

In order to specifically target a cancer-associated marker, Marnett and coworkers recently developed an indomethacin-based fluorescent probe that they called fluorocoxib A (LM-4777) [12], which specifically binds cyclooxygenase-2 (COX-2), an enzyme that is preferentially expressed in inflamed and neoplastic tissue. COX-2 is the inducible cyclooxygenase isoenzyme and is induced by cytokines, mitogens and growth factors. It has been found to be abundantly over-expressed both in inflamed and cancerous tissues of the colon [13], prostate [14], breast [15], pancreas [16], lung [17], and skin [18–21]. Therefore, fluorocoxib A has potential to be an effective molecular probe for early cancer detection as a marker of both inflammation and malignancy.

Most BCC tumors are characterized by an aberrant expression of genes involved in the hedgehog-signaling pathway, often caused by mutations induced by UV light [22]. One of these affected genes, Ptc1, is an inhibitor of hedgehog signaling and is the cause of Basal Cell Nevus Syndrome (BCNS), a rare disease in which over 90% of the patients develop multiple BCCs. Epstein, Tang and colleagues have demonstrated that celecoxib, a selective COX-2 inhibitor, was able to decrease the severity of carcinogenesis in a BCNS mouse model (PF14 mice), and in BCNS patients in a 60-patient clinical trial [23]. These findings corroborated previous studies that linked COX-2 activation to the development of skin cancer [19].

Here we report detection of non-melanoma skin cancer (NMSC) in mice by *in vivo* fluorescence imaging using the fluorocoxib A probe.

## Materials and Methods

### Animals

Animal work was carried out according to the guidelines for animal care of the National Institutes of Health, Stanford University and the Children's Hospital Oakland Research Institute (CHORI).

**Spontaneous BCC Mouse Model.** Ptc1<sup>+/-</sup> K14-Cre-ER2 p53<sup>fl/fl</sup> (PF14) mice were injected with 100  $\mu$ l of tamoxifen (1 mg/ml) for three consecutive days. At eight weeks of age, mice were given 4 GY of ionizing radiation. Typically, microscopic BCCs develop in this model at 5mo of age and visible BCCs develop between 7 to 9 months as previously described [22]. This served as our spontaneous BCC/NMSC

mouse model for our molecular imaging experiments. The dorsal hair of the mouse was removed using Nair (Church & Dwight Co., Ewing, NJ) 24 hours before injection of the molecular probe for imaging.

**BCC Allograft Mouse Model.** SCID Hairless Outbred (SHO) mice were purchased from Charles River Laboratories (Wilmington, MA). BCC allografts were generated by subcutaneous injection of BCC cells into the flanks of SCID hairless mice. The single suspension of BCC cells were either from a previously established BCC cell line or isolated from primary tumors of the PF14 mouse.

For the primary tumor allografts, spontaneous tumors from PF14 mice were sliced into small pieces and incubated in 0.5% collagenase (Gibco #17100-017) solution for 1 hour at 37°C. Cells were further dissociated by pipetting and passed through a 70  $\mu$ m cell strainer. Cells were collected by centrifugation and resuspended at 20,000 cell/ $\mu$ l. Equal amounts of cell suspensions were mixed with ice-cold Matrigel (BD, Franklin Lakes, NJ) and injected intradermally (ID) 100  $\mu$ l (10<sup>6</sup> cells) into the lower flanks (left and right) of SHO mice. Also, different amounts of cells (100, 500, 1000, and 1,000, 5,000, 10,000) were subcutaneously injected in different regions of the lower back area of SHO mice to analyze the sensitivity (number of cells) of this detection approach.

The allografts from a BCC cell line were generated using a previously immortalized cell line (BSZ) from PF14 tumors [24]. BSZ cells were maintained in BSZ medium, prepared with 154-CF medium (Cascade Biologics, Portland, OR) containing 1% penicillin and streptomycin, 2% heat-inactivated fetal bovine serum (FBS) and chelexed with Chelex Resin Chelating Ion Exchange Resin (Biorad Laboratories, Hercules CA) and calcium chloride (0.2 mM). After trypsinization BSZ cells were resuspended in PBS and 10<sup>6</sup> cells were subcutaneously injected into the flanks of SHO mice [25].

Tumor location was recorded using a digital camera and tumor growth was recorded over time with caliper measurement. Tumor volume is calculated using the formula  $L*W^2/2$  [26].

### Systemic Administration of Molecular Probe

The systemic solution of 1 mg/kg fluorocoxib A was formulated as described by Uddin et al. [12], consisting of DMSO (16%), EtOH (33%), propylene glycol (17%) and sterile PBS (34%). A fluorocoxib A solution (60  $\mu$ l) was injected retro-orbitally (ro) into mice that had been anaesthetized with 2% isoflurane.

### In Vivo Fluorescence Imaging

One week prior to imaging, mice were fed low-fluorescent chow (Harlan Laboratories, Indianapolis, IN). Anaesthetized (2% isoflurane) mice were imaged at different time points after injection of fluorocoxib A (30 min, 3 h, 5 h, 7 h, 25 h) with the CRi Maestro (Caliper Life Sciences, Alameda, CA) *in vivo* imaging system using the auto-exposure mode. Fluorocoxib A fluorescence signals were monitored at 10 nm windows from 500 to 800 nm using an excitation filter (503 to 555 nm) and a long-pass emission filter (580 nm). The fluorocoxib A fluorescence spectrum of the skin of each mouse strain was obtained by unmixing the autofluorescence, previously obtained from a non-injected P14 mouse or SHO mouse. The protocol generated was used to analyze the acquired image data. Fluorescence average signal (counts per second per mm<sup>2</sup>) was quantified over a region of interest (roi), corresponding to tumors, using Maestro software.

In a co-injection experiment, a LiCor800-equivalent probe (LM-5516) was used as a negative probe (non-COX-2 binding probe) in combination with fluorocoxib A. The two fluorescence spectra were

analyzed using the auto-exposure and sequential mode functions of the Maestro software. Autofluorescence was unmixed similarly as described above. Unmixed images are pseudo-colored red for fluorocoxib A (LM-4777) and blue for LM-5516.

### Histopathologic Analysis of Tissue Samples

Mice were euthanized at the appropriate endpoint after imaging, considering tumor stage and size. The mice were visually inspected and macroscopically-detectable tumors were collected for further analysis. The skin of the mouse was also compared with the fluorescence image obtained with Maestro, and regions of the skin presenting fluorescence are considered as possible microscopic tumor sites while regions of skin not presenting any fluorescence signal under a certain threshold were considered as possible negative controls.

After removal of tissue, samples were immersed in a 2% formaldehyde, 0.2% glutaraldehyde in PBS solution for at least one hour. The fixative was aspirated and sample washed with PBS twice (PBS aspirated after each washing). The sample was stained using a  $\beta$ -gal staining kit (Roche, cat #: 11828673001) overnight. The staining solution was then removed and the sample washed with a 3% DMSO in PBS solution two times (solution aspirated after each washing), washed with 70% ethanol three times (ethanol aspirated after each washing), and left in 70% ethanol. Samples were processed for paraffin block embedding, sectioning, and hemotoxylin and eosin (H&E) staining (Redwood Dermatopathology, Santa Rosa, CA) [22].

### Immunohistochemistry

Tissues were collected in 10% buffered formalin and were embedded in paraffin for preparation as 5- $\mu$ m tissue sections. All tissue sections were subjected to antigen retrieval in 0.1 mM Citric acid for 8 minutes, and were treated in 10%  $H_2O_2$  for 10 minutes to block endogenous peroxidase activity.

Immunohistochemical staining was performed using an affinity purified primary rabbit anti-mouse COX-2 antibody (Cayman Chemical, # 160126; 1  $\mu$ g/ml), which is detected using the ImmPRESS HRP anti Rabbit Ig (Peroxidase) Kit (Vector Laboratories, Burlingame, CA), and visualized with 3,3' diaminobenzidine tetrahydrochloride (DAB) (Invitrogen, Carlsbad, CA). Sections were counterstained with hematoxylin (Thermo Fisher Scientific, Waltham, MA).

## Results and Discussion

### In Vivo Detection of NMSC with the Fluorocoxib A Probe

We used the BCC allograft model for establishing the *in vivo* imaging procedure of NMSC with fluorocoxib A. Figure 1 shows time-lapse *in vivo* fluorescence imaging of allograft mice after co-injection of fluorocoxib A (LM-4777) and LiCor800-equivalent (LM-5516) probes. We observed that fluorocoxib A specifically bound to the two tumor sites in Figure 1, B–D. From Figure 1E, fluorocoxib A fluorescence signal was determined to peak at 3 to 5 hours post-injection. The non-targeting LM-5516 shows minimal accumulation in the tumor sites. This demonstrates the targeting specificity of the fluorocoxib A probe to skin tumors, and establishes that the optimal timeframe for imaging is 3 to 5 h post-injection. This corroborates well with previous reports on fluorocoxib A [12], and we therefore choose the 3 h post-injection timepoint for our *in vivo* fluorescence imaging experiments.

### In Vivo Fluorocoxib A Signal Level Experiments with the Allograft Mouse Model

We tested the sensitivity of fluorocoxib A in the BCC allograft mouse model. Different numbers of BCC cells (100, 500, 1000 and 1000, 5000, 10,000) were subcutaneously injected into SCID hairless mice. The mice were then subsequently injected with fluorocoxib A, retro-orbitally. Sites with 1000 BCC cells, or greater, were consistently detectable above background.

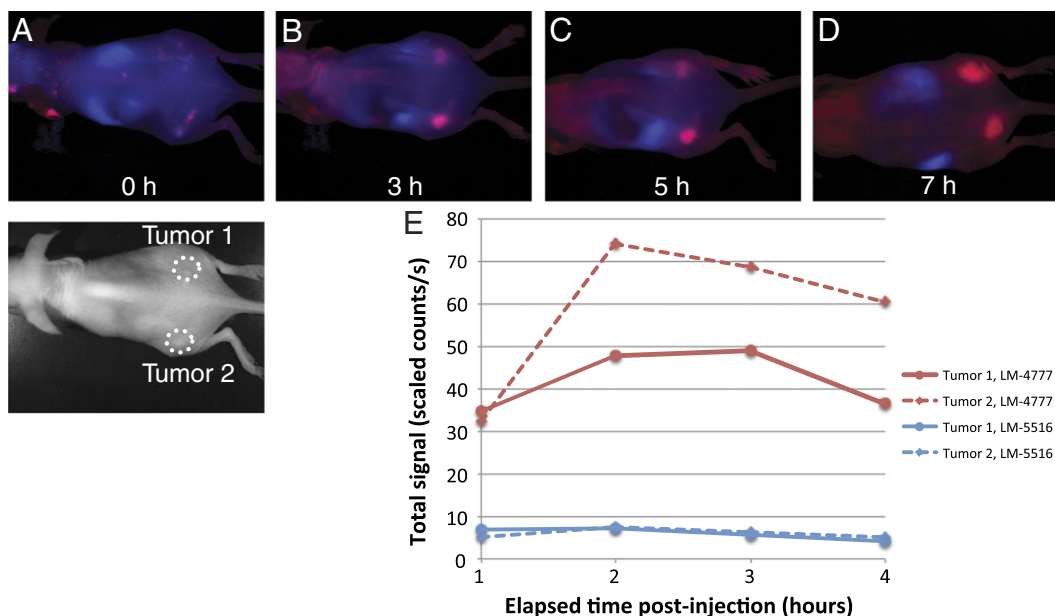


**Figure 1.** Specific targeting of tumor with fluorocoxib A and its imaging timecourse in the BCC allograft model. Time-lapse *in vivo* fluorescence imaging of BCC allograft mice after co-injection of Fluorocoxib A (LM-4777) and LiCor800-equivalent (LM-5516) probes. Time sequence is (A) 0 hours (B) 3 hours (C) 5 hours (D) 7 hours post-injection, where the allograft mouse is oriented as in the brightfield image below (A). The red signal represents LM-4777 and the blue signal represents LM-5516. (E) Total unmixed fluorescence signal of tumor 1 and 2 at each time point for LM-4777 and LM-5516.

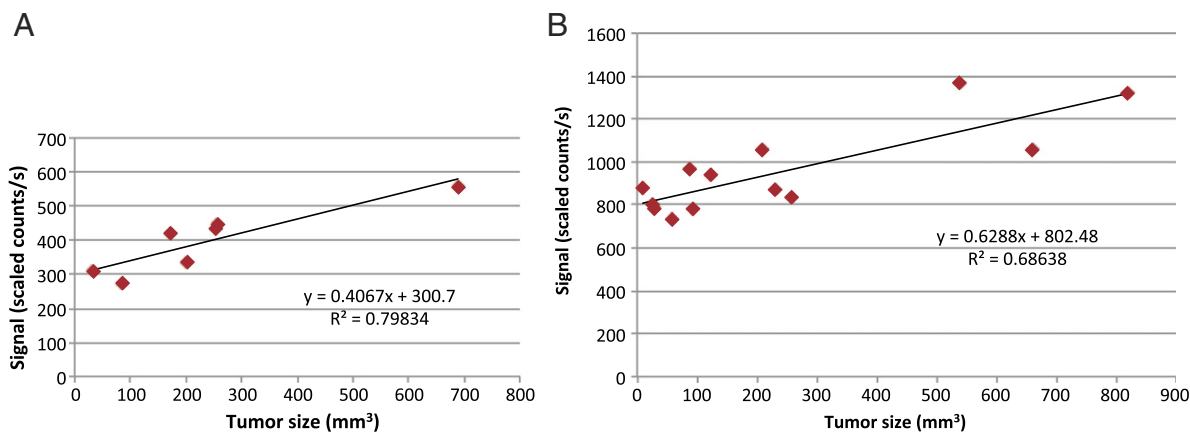


**Figure 2.** Linear relationship between fluorescence signal from fluorocoxib A and tumor volume in allograft models. Graphs of tumor size vs *in vivo* fluorescence signal for BCC allograft mice. (A) Allografts from BCC cell line (7 tumors from 4 mice). (B) Allografts from primary tumors (13 tumors from 7 mice).

The relationship between the fluorocoxib A signal level to the tumor size was investigated with two types of BCC allograft mice, one derived from a BCC cell line and one derived from primary tumors of the P14 mouse model. The fluorescence signal corresponding to each tumor mass is plotted in Figure 2, A and B, respectively. Allografts from the BCC cell line exhibit a better linear fit compared to the primary tumor derived allografts ( $R^2 = 0.80$  versus 0.69) which is most likely due to the cell population being more homogenous.

#### *In Vivo* Detection of NMSC in PF14 Spontaneous Mouse Model

P14 mice [22] that spontaneously develop BCC and SCC were imaged 3 h after systemic administration of fluorocoxib A via retroorbital injection. Threshold levels were set after unmixing the fluorescence spectra of the probe from the background, which mainly consists of autofluorescence of the skin. Then, tissue regions that were above threshold were harvested and processed for histologic analysis.

Visually discernable tumors are referred to as macroscopic tumors, while visually indiscernable tumors that look normal, but are later determined through histopathologic analysis to be small tumors are referred to as microscopic tumors. Figure 3 shows an *in vivo* imaging example and its corresponding representative histology. All the macroscopic tumors show fluorescence signal, while some other regions show signals above a threshold (Figure 3B) that visually present like normal skin. Both macroscopic tumors and potential microscopic tumor sites, along with control samples (below threshold signal) were harvested shortly after *in vivo* imaging. Microscopic BCCs were confirmed on sites such as region 3 in Figure 3B, through histologic analysis (Figure 3D), where microscopic tumors down to 100  $\mu\text{m}$  in size could be detected. We have analyzed skin containing 56 macroscopic fluorescent regions, 54 microscopic fluorescent regions, and 18 non-fluorescent regions ( $N = 9$  mice). The threshold size for histopathologically confirming microscopic tumors is set to

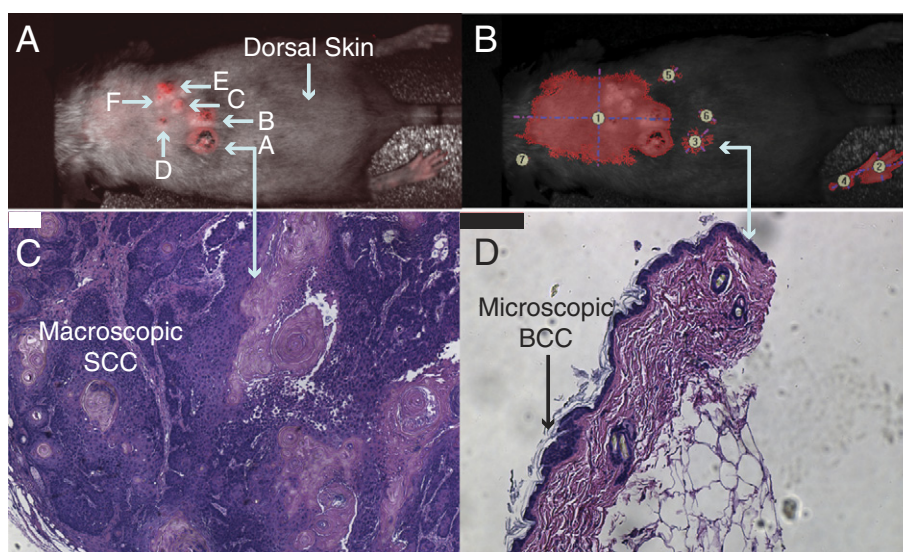


**Figure 3.** *In vivo* detection of macroscopic and microscopic NMSCs in the spontaneous P14 mouse model. (A) Fluorescence unmixed image (red), overlaid with brightfield image (grey), taken with Maestro. A–F refer to macroscopic visible tumors. (B) Fluorescence unmixed image that is thresholded and segmented (red), overlaid with brightfield image (grey), taken with Maestro. (C) Histology of macroscopic SCC, within region A of (A). (D) Histology of microscopic BCC, within region 3 of (B). The size of the scale bars is 100  $\mu\text{m}$ .

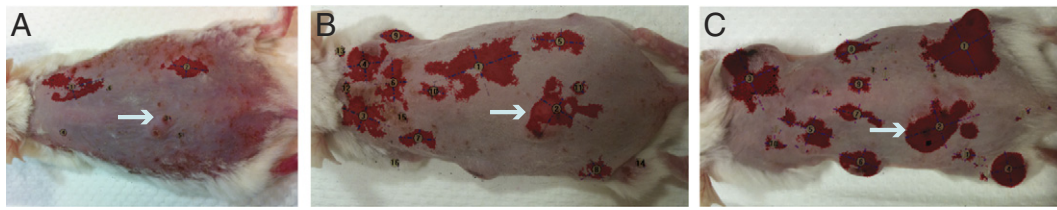


**Figure 4.** Sequential *in vivo* imaging of P14 mice shows development of macroscopic tumors. This is an overlay of the unmixed fluorescence image (thresholded) and color photograph of the same mouse corresponding to (A) Day 1, (B) Day 17, and (C) Day 27. Between Day 1 and Day 17, 3 macroscopic tumors developed from suspect ROIs (region of interest; potential microscopic tumor sites). Between Day 17 and Day 27, 7 macroscopic tumors emerge from suspect ROIs. The arrows follow tumor growth and corresponding fluorocoxib A signal of one region.

100  $\mu\text{m}$ . For macroscopic tumors, the sensitivity is 88% and specificity is 100%. For microscopic tumors, the sensitivity is 85% and specificity is 56%. Some false-negatives were attributed to areas that are adjacent to high-signal macroscopic tumors, which could

have overshadowed weak microscopic tumor signal. The lower specificity for microscopic tumors may be due to false positives resulting from interrogating a small subset of the imaged tissue region through histopathology. The sensitivity and specificity are dependent

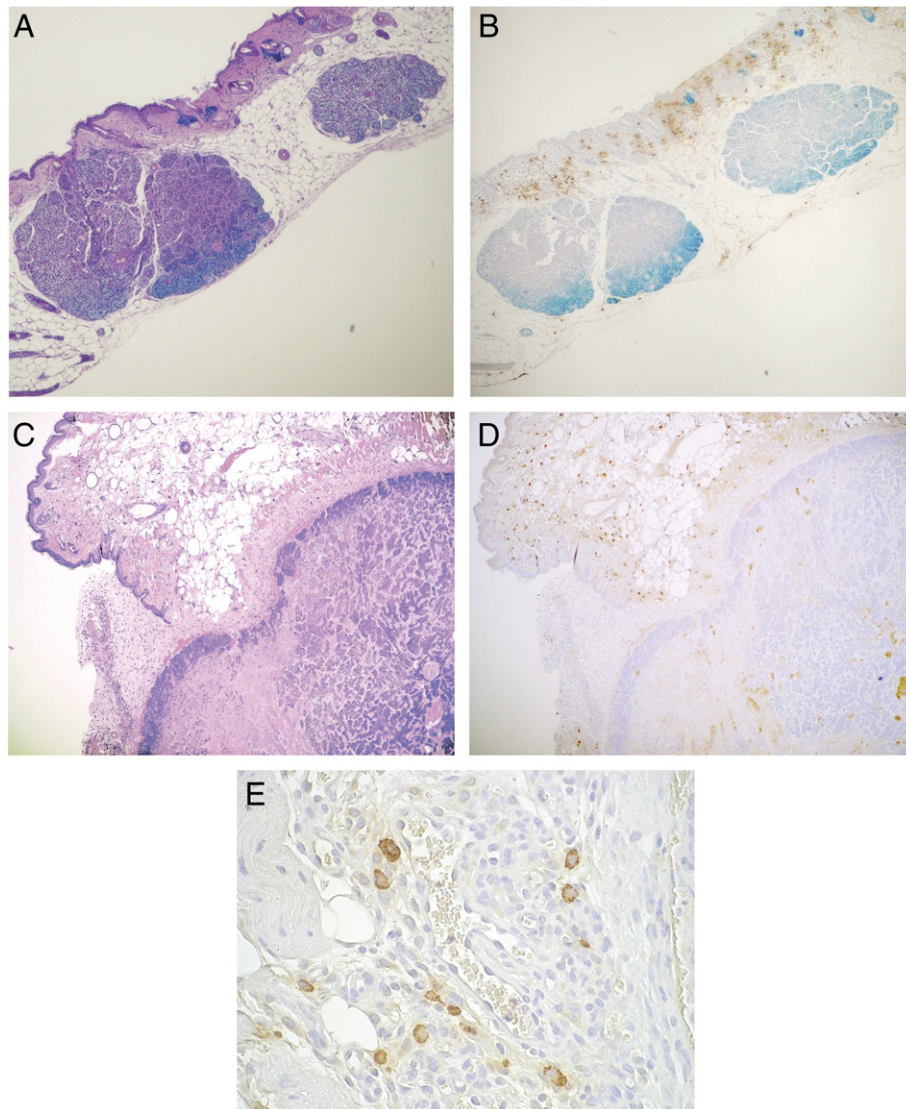


**Figure 5.** Immunohistochemical analysis of COX-2 expression. Two pairs of histology and immunohistochemistry slide images each taken from the same tissue block. Microscope images were taken at 4x magnification. (A) Histology image of a microscopic BCC in the P14 mouse model. (B) Immunohistochemistry of same tissue block as (A). (C) Histology image of a microscopic (indiscernible) metastatic BCC in the allograft mouse model. (D) Immunohistochemistry from same tissue block as (C). (E) 40  $\times$  magnification of a sub-area of (D) showing COX-2 expressing cells.

on the threshold signal setting that is set after the fluorescence unmixing stage, and the histologic threshold size that is set to determine microscopic tumors. This is especially the case with late stage transgenic P14 mice, which have numerous tumors developing throughout the skin surface. For human NMSCs, the development of tumors are more spatially separated, and therefore will be better suited for sensitive, early detection.

### Sequential *In vivo* Imaging of P14 Spontaneous Mouse Model to Track Tumor Development

We performed sequential *in vivo* imaging of the spontaneous tumor mice over time in order to track fluorescence signal and its correlation with tumor development. Figure 4 shows one mouse that was imaged over a period of four weeks. We observed 3 macroscopic tumors emerging from previous suspect 'regions of interest' (ROIs) between Day 1 and Day 17. The ROIs for each imaging time point were determined as regions emitting fluorescence signal above threshold. An additional 7 macroscopic tumors developed from suspect ROIs between Day 17 and Day 27. Overall, three mice were sequentially imaged, where 13 suspect ROIs (potential microscopic tumor sites) became macroscopic tumors while 3 ROIs did not develop into macroscopic tumors. This shows that fluorocoxib A signal is a good indicator for ROIs (that could already be microscopic tumor sites) that have a high probability of developing into macroscopic tumors in the future. This has implications for early detection and treatment that can be complemented with signal tracking of ROIs.

### Immunohistochemical Detection of COX-2 Expression

Histopathological classification and immunohistochemical analysis of COX-2 expression, shown in Figure 5, A and B, were performed on serial tissue sections from a microscopic BCC from the P14 spontaneous mouse model. COX-2 was predominantly expressed by cells within the dermal layer above the tumor. Figure 5, C and D show histologic and immunohistochemical analysis of a microscopic BCC on the back of the allograft mouse model. As shown in Figure 5, B and D, COX-2 was mainly expressed by stromal cells within the dermis and hypodermis overlying the tumors, with minimal expression of COX-2 in the epithelial cells of the tumor mass itself. As shown in Figure 5E, COX-2-positive cells exhibit a macrophage morphology, with predominantly cytoplasmic and perinuclear staining, a pattern consistent with the intracellular location of the COX-2 enzyme. These expression patterns are consistent with previous studies in human BCCs [19], colorectal tumors [27], and subdermal mammary tumor xenografts (unpublished observations) reporting COX-2 expression predominantly by infiltrating macrophages. One group has localized COX-2 expression to CD68-positive macrophages using dual-labeling immunofluorescence, and reported their proximity to capillaries [27]. These observations have led to the suggestion that COX-2 positive macrophages play a role in early tumor progression via the promotion of angiogenesis [27]. These reports along with our imaging data, show the potential of early detection of NMSC through sensitive and specific detection of COX-2 expressing cells.

### Conclusion

We have demonstrated *in vivo* detection of NMSC after systemic administration of fluorocoxib A that targets COX-2. Sensitive fluorescence imaging and analysis allows for detection of microscopic tumors that are visually undetectable otherwise. These results demonstrate the potential of fluorocoxib A as an effective *in vivo* imaging agent for early detection, margin delineation and guided biopsies of NMSCs.

### Acknowledgements

This work was supported, in part, by an unrestricted gift from the Chambers Family Foundation (CHC), by the Damon Runyon Clinical Investigator grant (JYT), and by grants from the National Institutes of Health U54 CA136465 (CHC), U54 CA136456 (CHC, BLK), CA128323-4,-5 (MJU), and CA89450 (LJM). Dr. Ra and Dr. Ali-Khan were supported, in part, during these studies by a grant from the Korean government and Catholic University Medical Center (CMC) in Seoul, Korea.

We thank Pauline Chu for immunohistochemistry. Imaging resources were supported by the Stanford Small Animal Imaging Service Center and the Stanford Cancer Institute.

### References

- [1] Rogers HW, Weinstock MA, Harris AR, Hincley MR, Feldman SR, Fleischer AB, and Coldiron BM (2010). Incidence estimate of nonmelanoma skin cancer in the United States, 2006. *Arch Dermatol* **146**, 283–287.
- [2] De Vries E, De Poll Franse V, Louwman WJ, de Gruijl FR, and Coebergh J (2005). Predictions of skin cancer incidence in the Netherlands up to 2015. *Br J Dermatol* **152**, 481–488.
- [3] Siegel R, Naishadham D, and Jemal A (2013). Cancer statistics. *CA Cancer J Clin* **63**, 11–30.
- [4] Perera E and Sinclair R (2013). An estimation of the prevalence of nonmelanoma skin cancer in the U.S. F1000Research; 2013.
- [5] Guy GP and Ekwueme DU (2011). Years of potential life lost and indirect costs of melanoma and non-melanoma skin cancer: a systematic review of the literature. *PharmacoEconomics* **29**, 863–874.
- [6] Pellacani G, Farnetani F, Gonzalez S, Longo C, Cesinaro AM, Casari A, Beretti F, Seidenari S, and Gill M (2012). In vivo confocal microscopy for detection and grading of dysplastic nevi: a pilot study. *J Am Dermatol* **66**, e109–e121.
- [7] Ulrich M, Roewer-Huber J, Bonzalez S, Rius-Diaz F, Stockfleth E, and Kanitakis J (2011). Peritumoral lefting in basal cell carcinoma: correlation of in vivo reflectance confocal microscopy and routine histology. *J Cutan Patol* **38**, 190–195.
- [8] Van Der Beek N, De Leeuw J, Demmendaal C, Bjerring P, and Neumann HAM (2011). PpIX fluorescence combined with auto-fluorescence is more accurate than PpIX fluorescence alone in fluorescence detection of non-melanoma skin cancer: An intra-patient direct comparison study. *Lasers Surg Med* **44**, 271–276.
- [9] Won Y, Hong SH, Yu HY, Kwon YH, Yun SJ, Lee SC, and Lee JB (2007). Photodetection of basal cell carcinoma using methyl 5-aminolaevulinate-induced protoporphyrin IX based on fluorescence image analysis. *Clin Exp Dermatol* **32**, 423–429.
- [10] Smits T, Kleinpenning MM, Blokx WAM, van de Kerkhof PCM, van Erp PEJ, and Gerritsen M-JP (2007). Fluorescence diagnosis in keratinocytic intraepidermal neoplasias. *J Am Dermatol* **57**, 824–831.
- [11] De Leeuw J, Van Der Beek N, Neugebauer WD, Bjerring P, and Neumann HM (2009). Fluorescence detection and diagnosis of non-melanoma skin cancer at an early stage. *Lasers Surg Med* **41**, 96–103.
- [12] Uddin MJ, Crews BC, Blobaum AL, Kingsley PJ, Gorden DL, McIntyre JO, Matrisian LM, Subbaramaiah K, Dannenberg AJ, and Piston DW, et al (2010). Selective visualization of cyclooxygenase-2 in inflammation and cancer by targeted fluorescent imaging agents. *Cancer Res* **70**, 3618–3627.
- [13] Maekawa MM, Sugano KK, Sano HH, Miyazaki SS, Ushiyama MM, Fujita SS, Gotoda TT, Yokota TT, Ohkura HH, and Kakizoe TT, et al (1998). Increased expression of cyclooxygenase-2 to -1 in human colorectal cancers and adenomas, but not in hyperplastic polyps. *Jpn J Clin Oncol* **28**, 421–426.
- [14] Gupta S, Srivastava M, Ahmad N, Bostwick DG, and Mukhtar H (2000). Over-expression of cyclooxygenase-2 in human prostate adenocarcinoma. *Prostate* **42**, 73–78.
- [15] Half E, Tang XM, Gwyn K, Sahin A, Wathen K, and Sinicrope FA (2002). Cyclooxygenase-2 expression in human breast cancers and adjacent ductal carcinoma in situ. *Cancer Res* **62**, 1676–1681.
- [16] Yip-Schneider MT, Barnard DS, Billings SD, Cheng L, Heilman DK, Lin A, Marshall SJ, Crowell PL, Marshall MS, and Sweeney CJ (2000). Cyclooxygenase-2 expression in human pancreatic adenocarcinomas. *Carcinogenesis* **21**, 139–146.
- [17] Hida T, Yatabe Y, Achiwa H, Muramatsu H, Kozaki K, Nakamura S, Ogawa M, Mitsudomi T, Sugiura T, and Takahashi T (1998). Increased expression of cyclooxygenase 2 occurs frequently in human lung cancers, specifically in adenocarcinomas. *Cancer Res* **58**, 3761–3764.

- [18] Buckman SYS, Gresham AA, Hale PP, Hruza GG, Anast JJ, Masferrer JJ, and Pentland APA (1998). COX-2 expression is induced by UVB exposure in human skin: implications for the development of skin cancer. *Carcinogenesis* **19**, 723–729.
- [19] An KP, Athar M, Tang X, Katiyar SK, Russo J, Beech J, Aszterbaum M, Kopelovich L, Epstein EH, and Mukhtar H, et al (2002). Cyclooxygenase-2 expression in murine and human nonmelanoma skin cancers: implications for therapeutic approaches. *Photochem Photobiol* **76**, 73–80.
- [20] Becker MR, Siegelin MD, Rompel R, Enk AH, and Gaiser T (2009). COX-2 expression in malignant melanoma: a novel prognostic marker? *Melanoma Res* **19**, 8–16.
- [21] Denkert C, Köbel M, Berger S, Siegert A, Leclere A, Trefzer U, and Hauptmann S (2001). Expression of cyclooxygenase 2 in human malignant melanoma. *Cancer Res* **61**, 303–308.
- [22] Wang GY, Wang J, Mancianti M-L, Epstein J, and Ervin H (2011). Basal Cell Carcinomas Arise from Hair Follicle Stem Cells in Ptch1 +/- Mice. *Cancer Cell* **19**, 114–124.
- [23] Kim J, Tang JY, Gong R, Kim J, Lee JJ, Clemons KV, Chong CR, Chang KS, Fereshteh M, and Gardner D, et al (2010). Itraconazole, a Commonly Used Antifungal that Inhibits Hedgehog Pathway Activity and Cancer Growth. *Cancer Cell* **17**, 388–399.
- [24] So P-L, Langston AW, Daniellina N, Hebert JL, Fujimoto MA, Khaimskiy Y, Aszterbaum M, and Epstein EH (2006). Long-term establishment, characterization and manipulation of cell lines from mouse basal cell carcinoma tumors. *Exp Dermatol* **15**, 742–750.
- [25] Wang GY, So P-L, Wang L, Libove E, Wang J, and Epstein EH (2011). Establishment of Murine Basal Cell Carcinoma Allografts: A Potential Model for Preclinical Drug Testing and for Molecular Analysis. *J Invest Dermatol*, 1–8.
- [26] Euhus DM, Hudd C, LaRegina MC, and Johnson FE (1986). Tumor measurement in the nude mouse. *J Surg Oncol* **31**, 229–234.
- [27] Chapple KS, Cartwright EJ, Hawcroft G, Tisbury A, Bonifer C, Scott N, Windsor ACJ, Guillou PJ, Markham AF, and Coletta PL, et al (2000). Localization of Cyclooxygenase-2 in Human Sporadic Colorectal Adenomas. *Am J Pathol* **156**, 545–552.